Interpretation of long-term measurements of radiatively active trace gases and ozone depleting substances

DECC contract number: GA0201

Quarterly Report (August - October 2012)

Date: 31st Oct 2012

Authors:
Alistair J. Manning (Met Office),
Simon O'Doherty, Aoife Grant (University of Bristol),
Dickon Young (Terra Modus)
Richard G. Derwent (rdscientific),
Peter Simmonds (INSCON)

Contents

1 Executive Summary

1.1 Project Summary

Monitoring of atmospheric concentrations of gases is important in assessing the impact of international policies related to the atmospheric environment. The effects of control measures on chlorofluorocarbons (CFCs), halons and HCFCs introduced under the 'Montreal Protocol of Substances that Deplete the Ozone Layer' are now being observed. Continued monitoring is required to assess the overall success of the Protocol and the implication for atmospheric levels of replacement compounds such as HFCs. Similar analysis of gases regulated by the Kyoto Protocol on greenhouse gases will likewise assist policy makers.

Since 1987, high-frequency, real time measurements of the principal halocarbons and radiatively active trace gases have been made as part of the Global Atmospheric Gases Experiment (GAGE) and Advanced Global Atmospheric Gases Experiment (AGAGE) at Mace Head, County Galway, Ireland. For much of the time, the measurement station, which is situated on the Atlantic coast, monitors clean westerly air that has travelled across the North Atlantic Ocean. However, when the winds are easterly, Mace Head receives substantial regional scale pollution in air that has travelled from the industrial regions of Europe. The site is therefore uniquely situated to record trace gas concentrations associated with both the mid-latitude Northern Hemisphere background levels and with the more polluted air arising from Europe.

The observation network in the UK has been expanded to include three additional stations; Angus Tower near Dundee, Tacolneston near Norwich and Ridge Hill near Hereford. Ridge Hill became operational in February 2012, Tacolneston began operating in July 2012 and Angus Tower has been making measurements since late 2005.

The Met Office's Lagrangian atmospheric dispersion model, NAME (**N**umerical **A**tmospheric dispersion **M**odelling **E**nvironment), has been run for each 2-hour period of each year from 1989 so as to understand the recent history of the air arriving at Mace Head at the time of each observation. By identifying when the air is unpolluted at Mace Head, i.e. when the air has travelled across the Atlantic and the air concentration reflects the mid-latitude Northern Hemisphere baseline value, the data collected have been used to estimate baseline concentrations, trends and seasonal cycles of a wide range of ozone-depleting and greenhouse gases for the period 1989-2012 inclusive.

By removing the underlying baseline trends from the observations and by modelling the recent history of the air on a regional scale, estimates of UK, Irish and North West European (UK, Ireland, France, Germany, Denmark, the Netherlands, Belgium, Luxembourg) emissions and their geographical distributions have been made using InTEM (Inversion Technique for Emission Modelling). The estimates are presented as yearly averages and are compared to the UNFCCC inventory.

The atmospheric measurements and emission estimates of greenhouse gases provide an important cross-check for the emissions inventories submitted to the United Nations Framework Convention on Climate Change (UNFCCC). This verification work is consistent with good practice guidance issued by the Intergovernmental Panel on Climate Change (IPCC).

2 Overview of Progress

The Mace Head observation station continues to operate effectively and there are no data issues to report.

The noise in the Ridge Hill N_2O and SF_6 observations has been significantly reduced.

Tacolneston is now operational.

Tall Tower Angus observations are under review. Issues still remain before the observations can be used.

Atmospheric baseline concentrations for each gas reported at Mace Head have been estimated through to the end of August 2012 and the website updated.

Web site officially launched.

InTEM (INversion Technique for Emission Modelling) has been improved.

3 Operational sites and gases monitored

Instruments	Mace Head – MHD		Analysis Freq. Air	Tall Tower Angus - TTA	Analysis Freq. Air
Picarro	CO_2 CH_4 (Also on GC-MD)		1 min/hourly avg	CO_2 (coming soon) CH_4 (coming soon)	1 min/hourly avg
LiCor	CO_2 (historic data, pre 2011)		1 hour avg	CO_2	30 min avg
GC-ECD	N_2O CFC-12 CFC-11 CFC-113	$CHCl_3$ CH_3CCl_3 CCl_4	40 mins	N_2O SF_6	1 hr
GC-FID	CH_4		40 mins	CH_4	1 hr
RGA3	H_2 CO		40 mins	H_2 CO	1 hr
Medusa	SF_6 CF_4 C_2F_6 C_3F_8 c-C_4F_8 HFC-23 HFC-32 HFC-134a HFC-152a HFC-125 HFC-143a HFC-227ea HFC-236fa HFC-43-10mee HFC-365mfc HFC-245fa HCFC-22 HCFC-141b HCFC-142b HCFC-124	CFC-11 CFC-12 CFC-13 CFC-113 CFC-114 CFC-115 H-1211 H-1301 H-2402 CH_3Cl CH_3Br CH_3I CH_2Cl_2 CH_2Br_2 $CHCl_3$ $CHBr_3$ CCl_4 CH_3CCl_3 $CHCl=CCl_2$ $CCl_2=CCl_2$	2 hrs		

Table 1: Operational sites, instrumentation and gases monitored.

Instruments	Tacolneston – TAC		Ridge Hill - RHL	Analysis Freq. Air
Picarro	CO_2 CH_4		CO_2 CH_4	1 min/hourly avg
GC-ECD	N_2O SF_6		N_2O SF_6*	20 mins
PP1	H_2 CO			20 mins
Medusa	CF_4 C_2F_6 C_3F_8 c-C_4F_8 HFC-23 HFC-32 HFC-134a HFC-152a HFC-125 HFC-143a HFC-227ea HFC-236fa HFC-43-10mee HFC-365mfc HFC-245fa HCFC-22 HCFC-141b HCFC-142b HCFC-124 CFC-11	CFC-12 CFC-13 CFC-113 CFC-114 CFC-115 H-1211 H-1301 H-2402 CH_3Cl CH_3Br CH_3I CH_2Cl_2 CH_2Br_2 $CHCl_3$ $CHBr_3$ CCl_4 CH_3CCl_3 $CHCl=CCl_2$ $CCl_2=CCl_2$		2 hrs

Table 2: Operational sites, instrumentation and gases monitored.

.

4 Update on three UK sites

4.1 Angus Tower

The GC-ECD at Angus Tower (TTA), which measures N_2O and SF_6, was previously operating with problems (and a very high background signal). The ECD detector was replaced in December 2011. The new detector gave a low background and data quality improved for N_2O and SF_6. Very recent N_2O data appears to overlay well with Mace Head measurements (with a constant baseline offset) (Figure 1). From visual inspection the SF_6 data overlays well with Mace Head data. The CH_4 data overlays well with Mace Head data but the magnitude of pollution events is smaller at Angus than Mace Head. Possible reasons for this are that the line is contaminated with algae, which may consume CH_4 (or N_2O). Or because Angus samples are taken from 185 m up the tower and at this height the pollution events are diluted. CO_2 data generally overlays well with Mace Head data however there appear to be many recent depletions in CO_2 which are not seen at Mace Head.

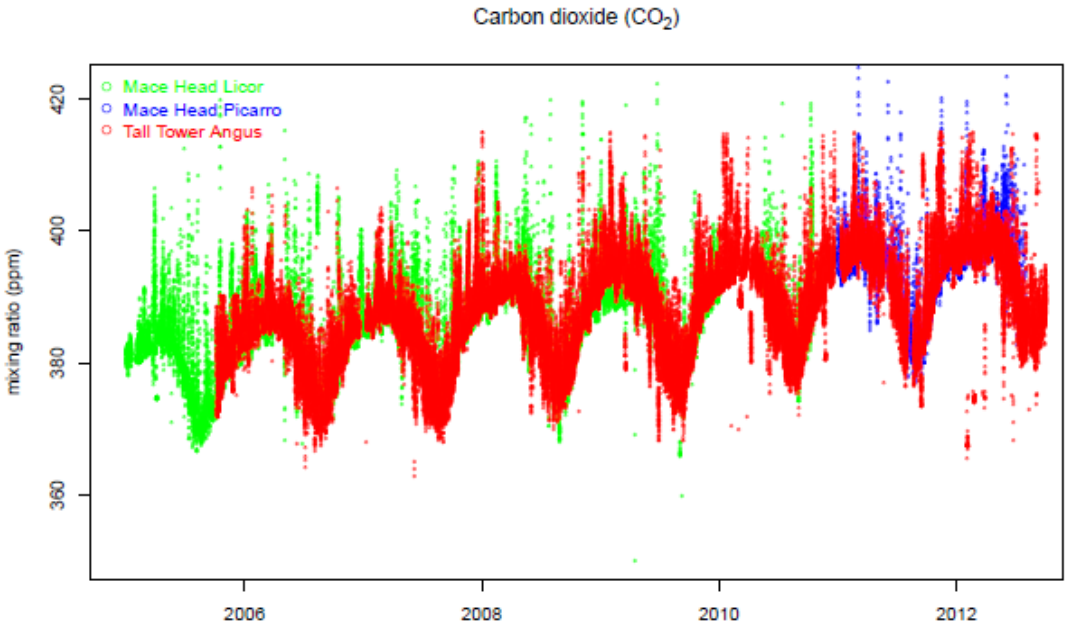

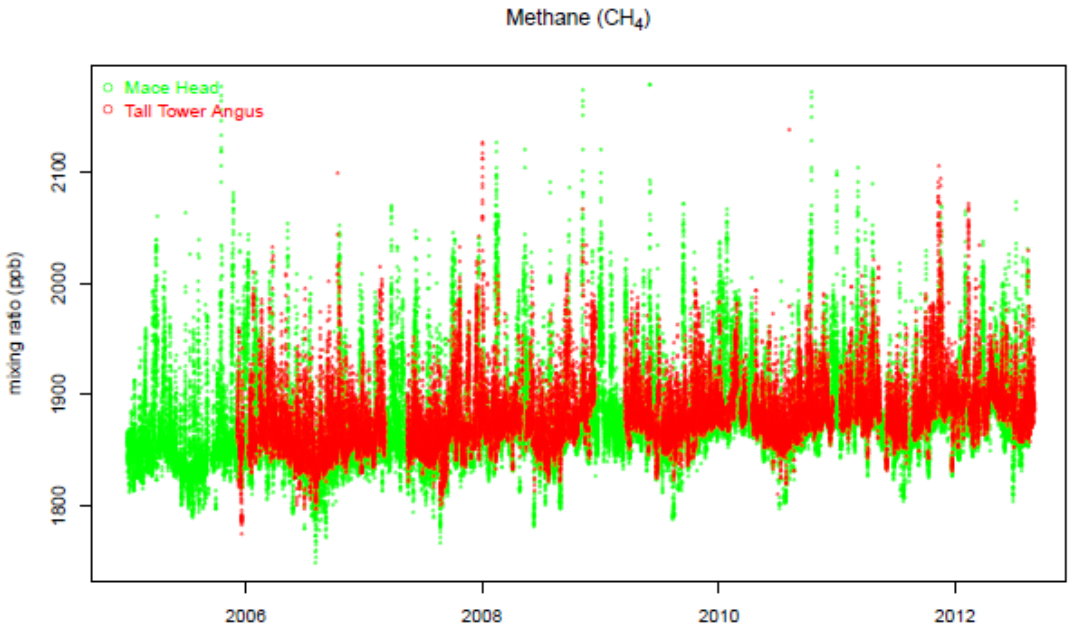

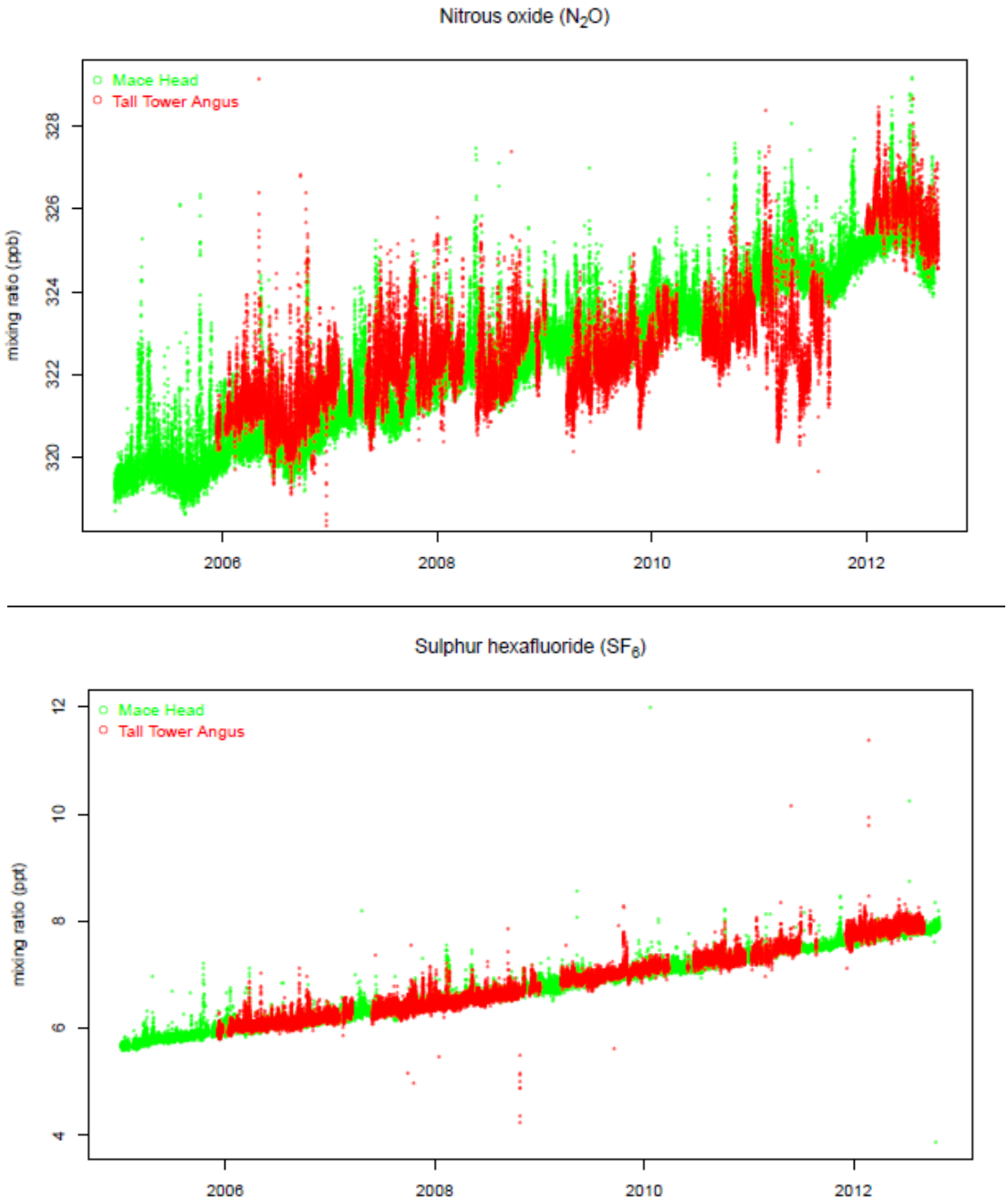

Figure 1: Angus,Tower and Mace Head data for CO_2, CH_4, N_2O and SF_6.

4.2 Tacolneston

The Mobile lab was craned onto site on the 23rd of July 2012, equipment was installed by the team from Bristol University on the 24th/25th of July when internet and electricity was also installed to the cabin. The internet connection was not activated until the 22nd of August although data was being collected during this entire period. There were leaks of carrier gas for the MD instrument and a regulator leak of the Medusa standard so on the 3rd/4th/5th of September a site visit was made by Aoife Grant to resolve these problems. The precision of the Tacolneston Medusa does not yet match that of the Mace Head Medusa. It is thought that a new ion-source and electron multiplier are required, these part have now been ordered and received A site visit is planned for the 1st/2nd of November by Simon O'Doherty to install new parts to the mass-spectrometer with the aim of improving instrument precision. Comparisons of the ambient record with associated standard precision are shown in Figure 2 (a)-(f).

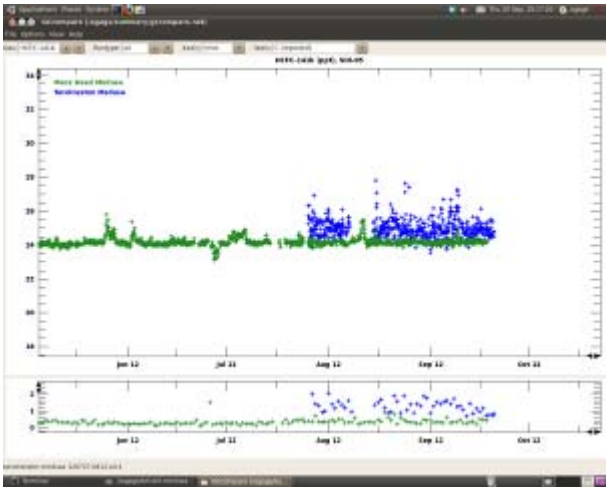

Figure 2: (a) HCFC-141b

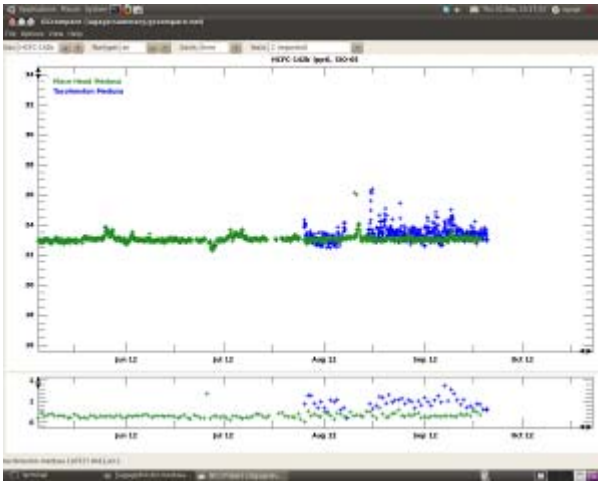

(b) HCFC-142b

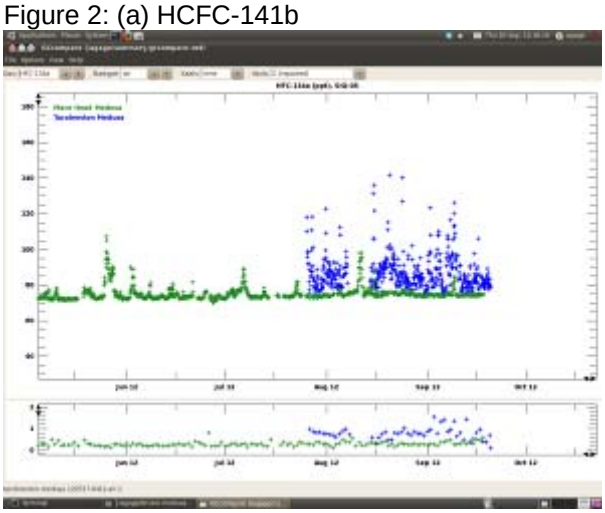

(c) HFC-134a

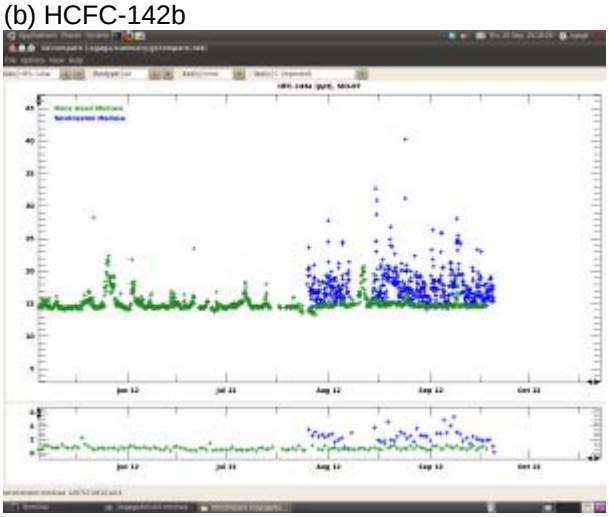

(d) HFC-143a

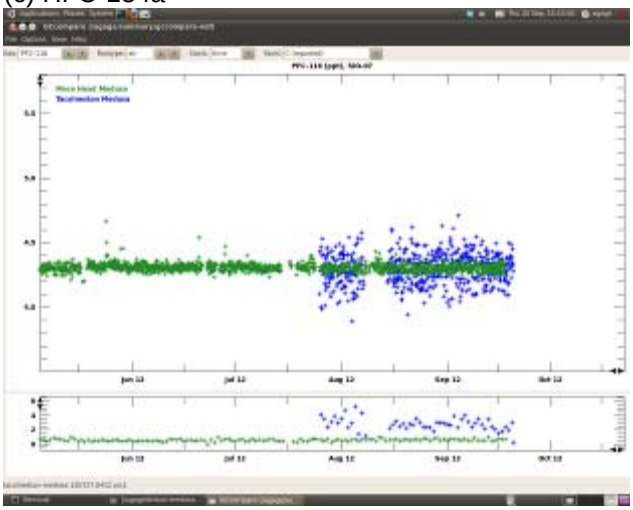

(e) PFC-116

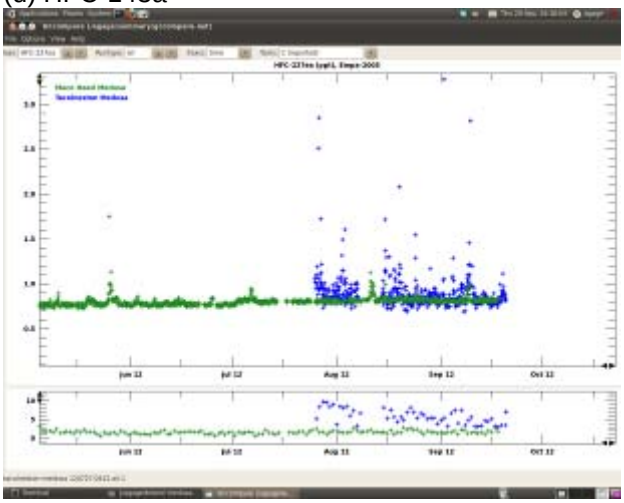

(f) HFC-227ea

Carrier gas (Ar/CH_4) for the MD system for the N_2O and SF_6 channel was found to be contaminated resulting in no measurements of SF_6 and N_2O from the 9th to the 29th of October. This has now been resolved. A plot overlaying SF_6 data acquired by the Medusa and MD at Tacolneston demonstrate the excellent agreement obtained between the 2 instruments (Figure 3).

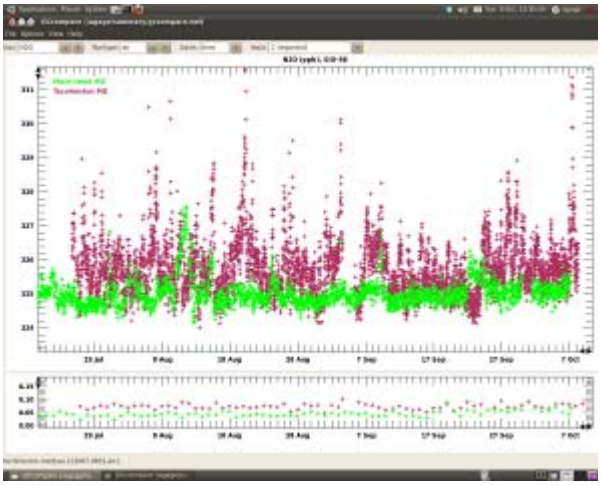

Figure 3: (a) N_2O at Mace Head (green) and Tacolneston (purple)

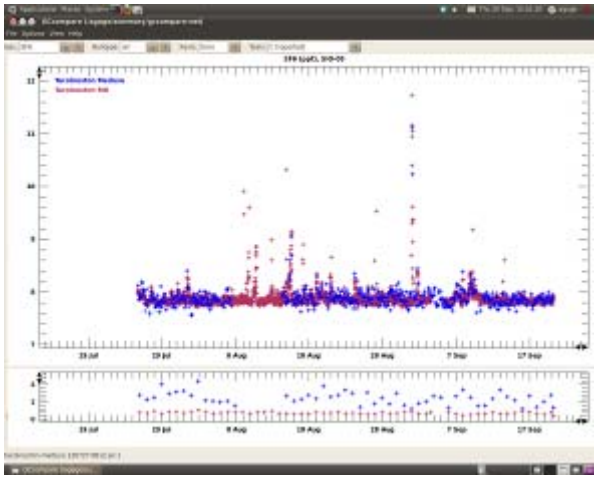

(b) Comparison of Tacolneston SF_6 on the GCMD (purple) vs Medusa (blue).

4.3 Ridge Hill

The Picarro Cavity Ring Down Spectrometer (CRDS) has generally been running well at Ridge Hill. The CRDS was installed on the 23rd of February. The CRDS began running air from the two tower heights of 45 m and 90 m, alternating every 30 minutes and running the target tank at 20 hour intervals. The target tank ran out and was replaced by an interim target on the 11th of July. The normal target was sent to MPI Jena for refilling, returned and replaced on the instrument on the 30th of August. Data is being transferred every day to the ICOS (Integrated Carbon Observation System) for processing and calibrated data returned daily to the data server held at Bristol University.

The GC-ECD at Ridge Hill has generally been running well in the last quarter. As highlighted in the last quarterly report, modifications were made on the 11th of July to improve instrument precision. Temperature stability was improved by addition of extra insulation around the instrument as the lab is not air-conditioned. A larger sample loop was also added. Both these changes resulted in improvement of N_2O precision to 0.1-0.15% and 1.0-1.5% for SF_6.

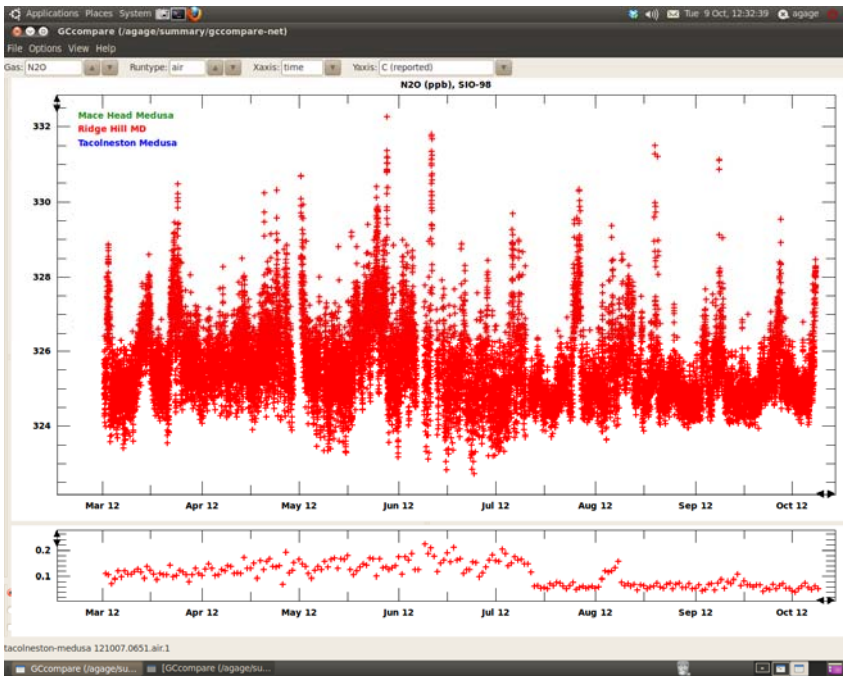

Figure 4: Improvement in sample precision (bottom plot) and its effect on the ambient N_2O data record (top plot).

A carrier gas cylinder fitted to this instrument on the 4th of July was found to be contaminated with a small quantity of SF_6 resulting in loss of SF_6 data capture from the 4th to the 18th of July. N_2O data was not affected by this. A regulator to test new carrier gas cylinders was fitted outside with a line running into the

cabin and instrument on the 8th of August. This will be used in future to test for contamination of carrier gas cylinders before it is used on the instrument, thus preventing possible loss of data.

A cover was made for the external gas bottle rack that holds the carrier gas outside the cabin and fitted on the 18th of September. This is to prevent weathering of the carrier gas cylinders but more importantly the regulators.

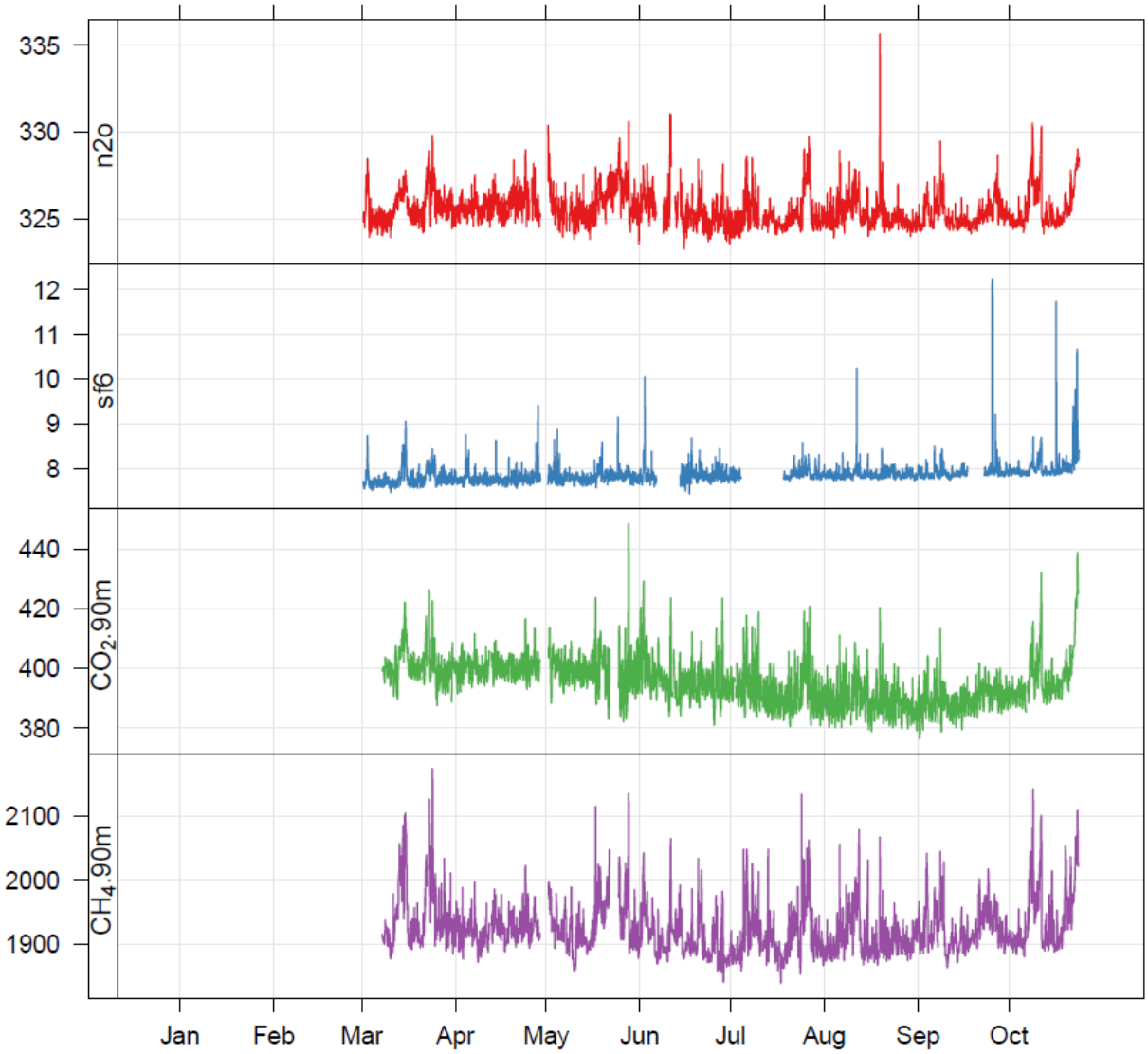

Figure 5: Ridge Hill data during 2012 for CO_2, CH_4, N_2O (reported in ppb) and SF_6 (reported in ppt) at the 90 meter sampling height.

5 Modelling

5.1 Baseline Mass Mixing Ratios

For each gas observed at Mace Head, Ireland, a baseline analysis has been performed for the period Feb. 1989 to Sept. 2012 where observations are available. The details of the method can be found in Manning *et al*, 2011. A selection of the Northern Hemisphere baseline analysis figures that appear on the website (www.metoffice.gov.uk/atmospheric-trends) are shown in the following section. For each gas, the monthly/annual baseline mass mixing ratios, growth rates, and seasonal cycles over the entire record at Mace Head are shown.

Work has been undertaken to understand the uncertainty in estimating the baseline growth rate and the seasonal cycles. Working with the estimated hourly baseline values the time-series is split into 2 separate components, a long-term trend and a residual or seasonal cycle component. Three different methods have been investigated to estimate these features.

5.1.1 Method 1 (RA)

This is the most basic method and is a simple 12-month running average. At each hour in the time-series calculate the 1-year average of the baseline mass mixing ratios centred on this hour (y_{mc}). This is the long-term trend component, subtracting this from the actual hourly baseline estimate at this time (y_c) gives the residual (r_c).

y_{mc} = Yearly-averaged baseline value at current time.

$$r_c = y_c - y_{mc}$$

5.1.2 Method 2 (Q5)

At each hour calculate the 1-year average centred on this hour. For the five year period centred on this hour calculate the quadratic line (eq. 1), using standard value decomposition, that best-fits (minimises difference between time-series y_m and y_a) five years of hourly data, each a yearly averaged value. The baseline value estimated at the current hour using this best-fit line (y_{mc}) is the long-term trend value at this hour, the residual component (r_c) is found by subtracting this value from the actual hourly baseline estimate at this time (y_c).

$$y_m = a + bt + ct^2, \quad where, \quad t = time \qquad \ldots(1)$$

y_a : Year-averaged baseline values over five years (hourly)

Find *a*, *b*, and *c* that minimises difference between y_m and y_a, then calculate y_{mc},

$$r_c = y_c - y_{mc}$$

5.1.3 Method 3 (Q2H)

At each hour calculate the 1-year average centred on this hour. For the two year period centred on this hour calculate the best-fit line (minimises difference between time-series y_m and y_e), using a function that has a quadratic and harmonic component (eq. 2). The best-fit line will use two years of hourly baseline data. The value estimated at the current hour using the quadratic component of the best-fit line (y_{mc}) is the long-term trend value at this hour, the residual component (r_c) is found by subtracting this value from the actual hourly baseline estimate at this time (y_c).

$$y_m = a + bt + ct^2 + d.\sin(2\pi t) + e.\cos(2\pi t) + f.\sin(4\pi t) + g.\cos(4\pi t), \; where \; t = time \; \ldots(2)$$

y_e : Baseline values over two years (hourly)

$$y_{mc} = a + bt + ct^2, \quad where, \quad t = current \; hour$$

$$r_c = y_c - y_{mc}$$

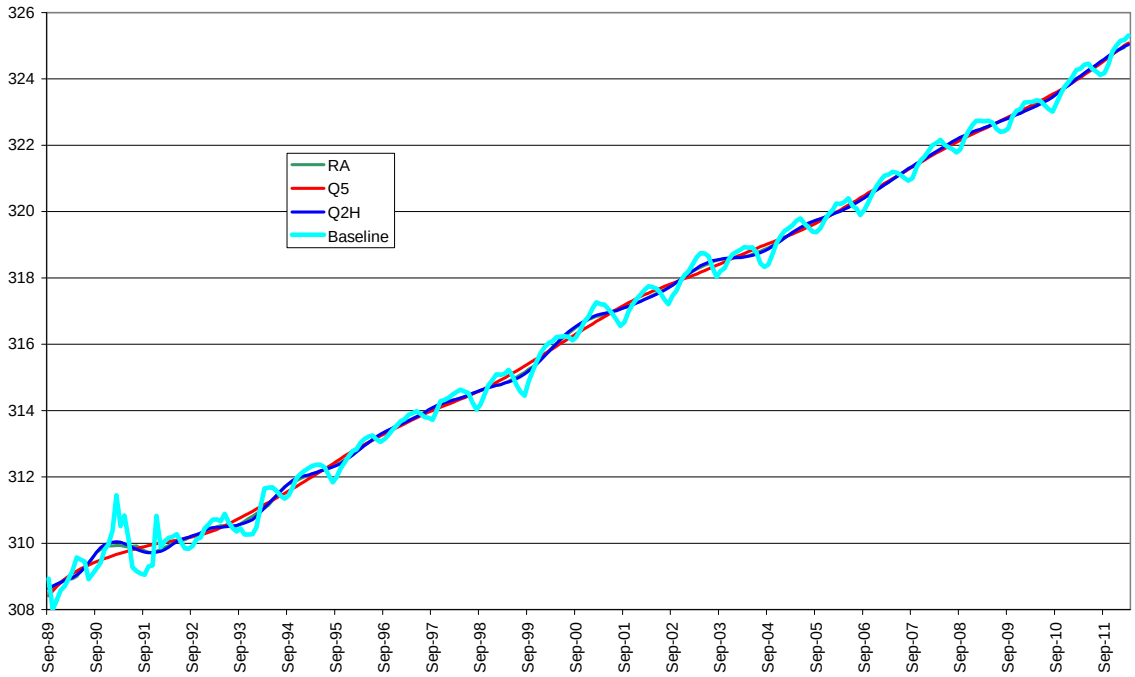

Figure 6: N_2O baseline (light blue) mass mixing ratios (ppb) with three trend lines from the three methods.

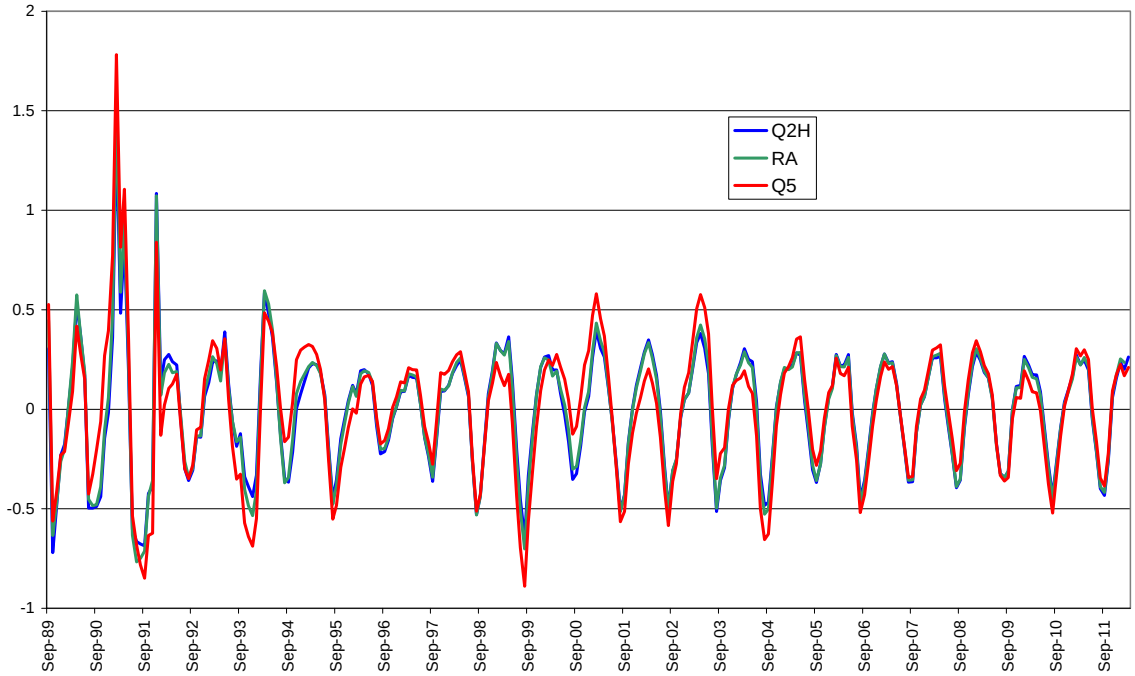

Figure 7: Estimated residual (seasonal signal) mass mixing ratios (ppb) for N_2O from the three methods.

Figures 6 and 7 show the results for N_2O from the application of the three methods. Each of the methods are broadly similar although there are subtle differences. The method Q5 is the most distinct although the differences are small.

5.2 Baseline Growth Rate

An important quantity to estimate is the growth or decline of the mass mixing ratios of each gas observed. This is estimated using the long-term trend values and calculating the local slope of this time-series. For each day calculate the average long-term trend from the hourly values. Using the current, previous and next daily trend values calculate the linear polynomial that best-fits these three quantities. The slope of this line is the growth rate for the current day. In previous reports the current long-term trend value minus the value from the same time the previous year was used as the current yearly growth rate. This has the

problem of not being responsive to recent changes and is dependent, by its very nature, on what was occurring in the previous year.

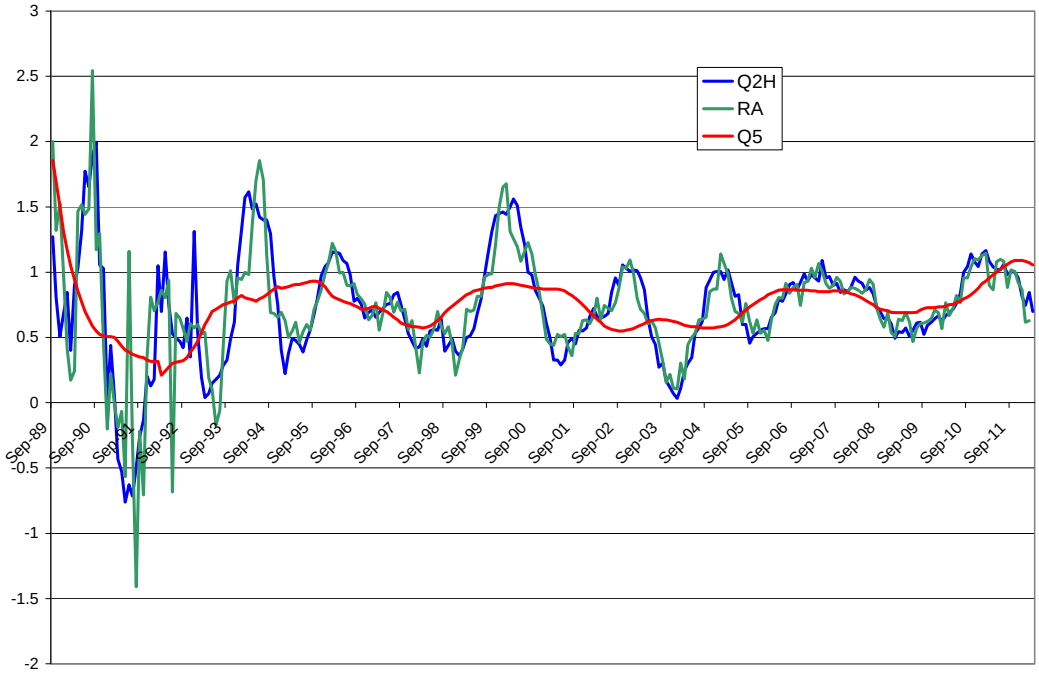

Figure 8: Growth rates (ppb/yr) for N_2O using the three different methods.

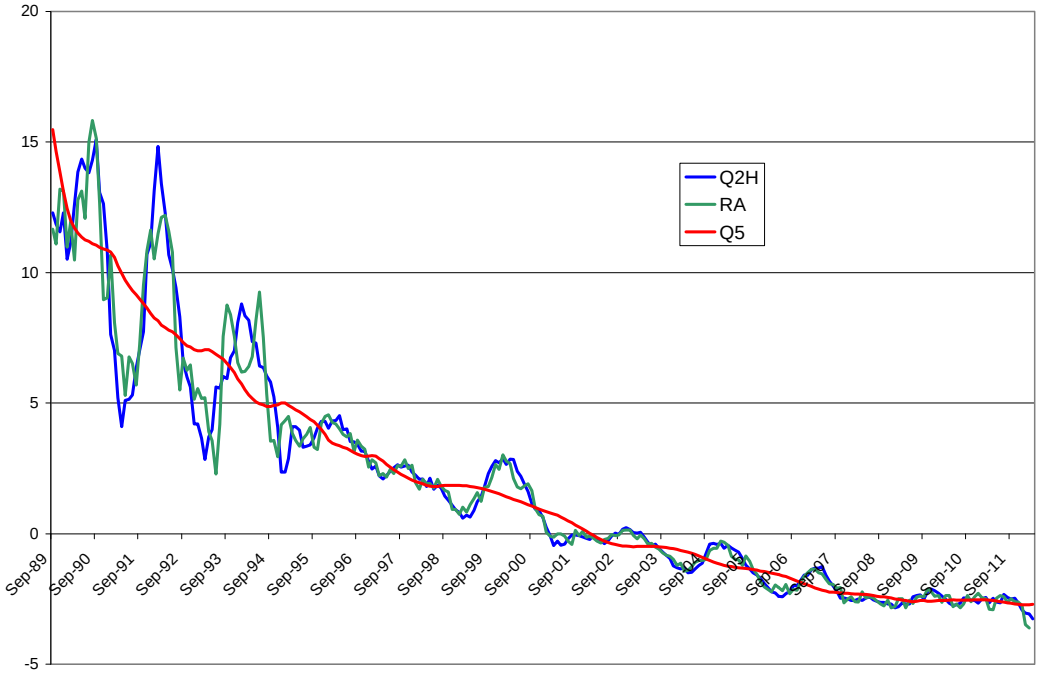

Figure

Figure 9: Growth rates (ppt/yr) for CFC-12 using the three different methods.

Figures 8 and Figure 9 show the growth rates estimated using the three different methods when applied to N_2O and CFC-12 respectively. As expected the five year quadratic method (Q5) is considerably smoother than the other 2 methods. The simple 1-year running average method (RA) is the least smooth.

In previous reports method Q5 was used to estimate the growth rate and seasonal cycles. It is proposed that the growth rate and seasonal cycle estimates should be calculated using method Q2H as has been done for the data in the next section of this report. This method is more responsive than method Q5 to current changes but is smoother than the more simplistic method RA. There is no definitive answer as any one of the three methods could be used. Also these three methods were chosen to be representative as there are numerous other options and time-periods that could be used. Each of the methods presented give broadly similar answers so the underlining results are unchanged.

5.3 Inversion Grid

Within the inversion system, InTEM, the basic core grid resolution of the maps is approximately 25 km. In order to balance the contributions from different regions these core grid boxes need to be grouped together as the distance from the observation point increases. In previous studies the grids have been grouped into 2x2, 4x4, 8x8, 16x16 and 32x32 larger grids. However this grouping takes no account of country borders therefore different countries will appear under the same large grid box, see Figure 10. This grouping has been improved so that the grouping ultimately conforms to the country borders. The grids are now limited by these country borders (regions) of specific interest. Figure 11 shows extent of each of these large regions; each region is independently coloured (the actual colour is irrelevant). These large regions are sub-divided into smaller domains depending on the amount of information each region contributes to the observation point. Figure 12 shows the outcome of the new gridding process. Note that the country borders are extended into the surrounding seas and oceans to ensure a country's emissions are fully captured.

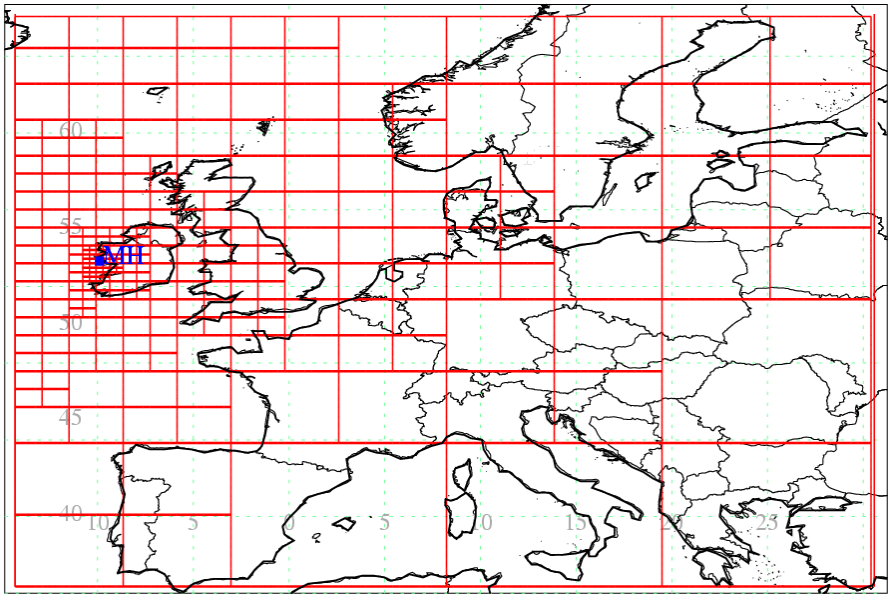

Figure 10: Grid resolution from old system for a 3-year inversion period with Mace Head observations.

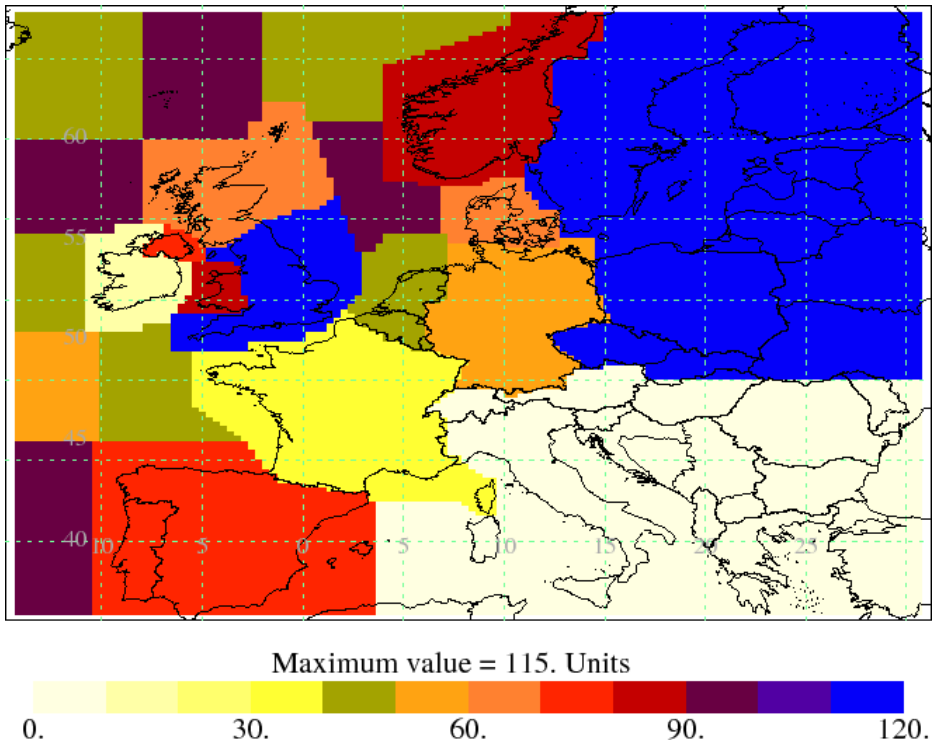

Figure 11: Extent of the large regions used to define the new inversion grid

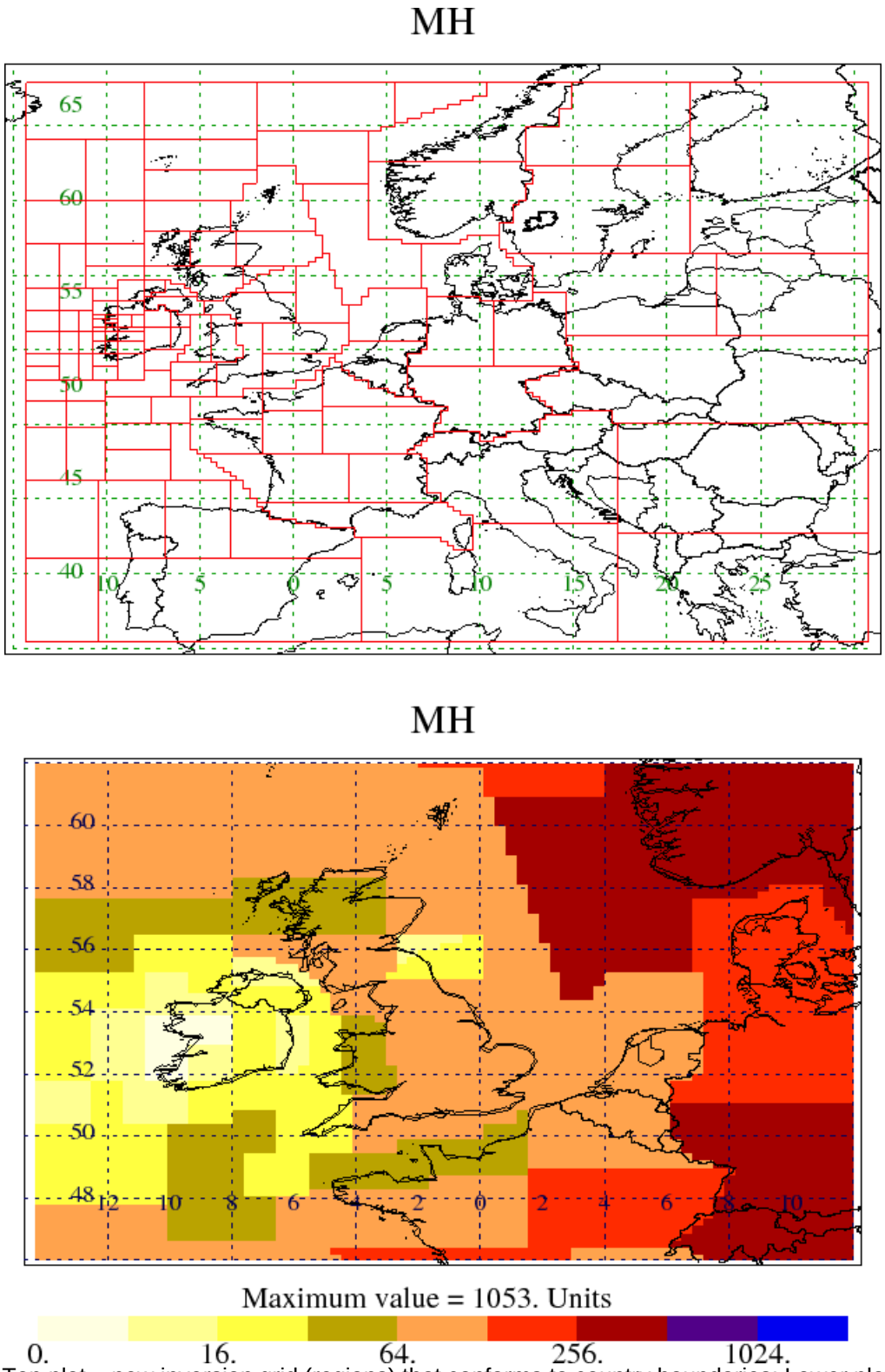

Figure 12: Top plot – new inversion grid (regions) that conforms to country boundaries; Lower plot – the number of core basic grids in each of the inversion regions.

The results of the inversion for methane using the new and old grid methods are shown in Figures 13 and 14 respectively. The black lines in the two plots are very similar demonstrating that the new gridding system has not had a detrimental impact on the inversion process. It does however allow a cleaner distinction between different countries and this will be important when emissions are estimated from the Devolved Administrations (DAs).

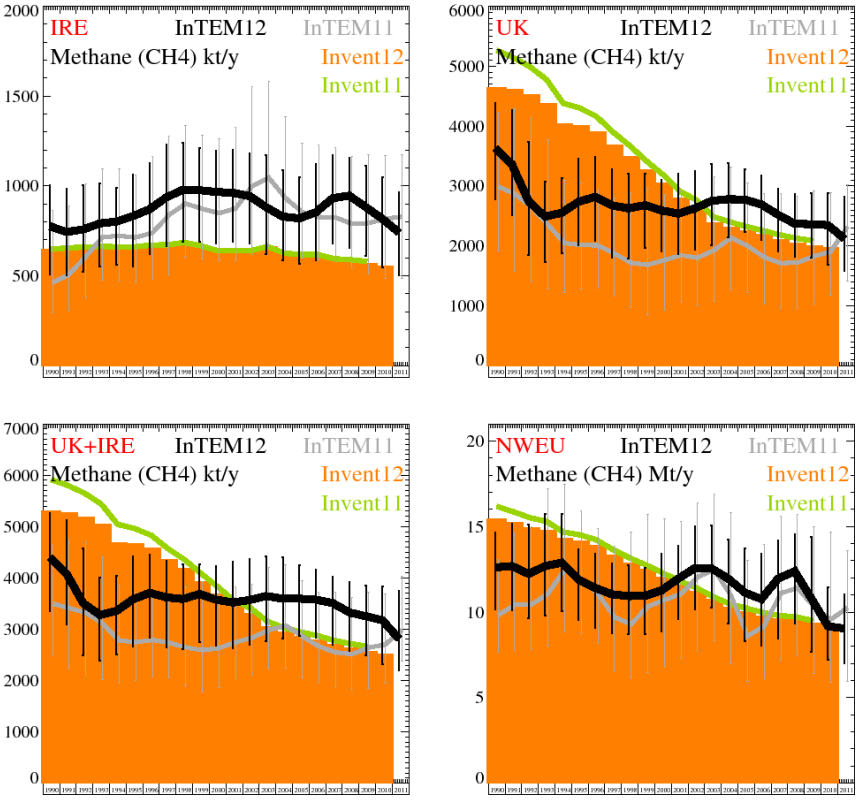

Figure 13: 3-yr inversion results for CH4 using the old grid (black line). The grey line denotes the inversion results from the last annual report (March 2012). The orange and green lines show the inventory estimates submitted in 2012 and 2011 respectively.

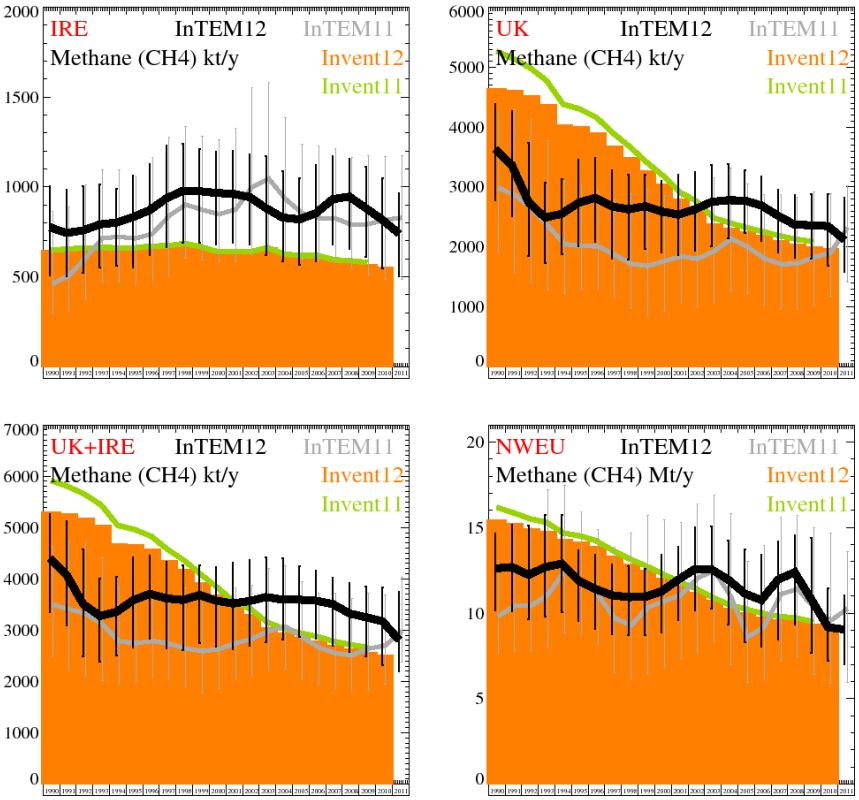

Figure 14: 3-yr inversion results for CH4 using the new grid (black line). The grey line denotes the inversion results from the last annual report (March 2012). The orange and green lines show the inventory estimates submitted in 2012 and 2011 respectively.

6 Improvements to InTEM (April 2012 – October 2012)

1. Below baseline observations not fixed to zero

Previously any observation that was below baseline, leading to a negative perturbation above baseline, was assigned a value of zero. This was because only the perturbation was available within the cost function routine. This has been altered so that the baseline is now also available. This means that the 2-hourly averaged observations can now be directly compared to the modelled deviations + estimated baseline, thereby removing the need for this zeroing step. The size of these negative deviations therefore now impact on the skill score assigned to each modelled emission map.

2. Each observation has an individual uncertainty

The uncertainty (+/- about the mean baseline) associated with each modelled observation is now available. This means that the uncertainty can change over the measurement period. Currently this uncertainty is limited to the uncertainty in the baseline within a time window (6-months) centred on the current time, but in time it will be expanded to include other factors such as; variable observational uncertainty, uncertainty per station, model transport uncertainty.

3. Alternate cost function has been developed

The distance of model time-series from the observations, outside of the baseline uncertainty, is a good measure of the quality of the current emission map and fully takes into account the allowable uncertainty at each observation time. Any modelled value that lies within the uncertainty is considered to be perfect and does not contribute to the cost of the emission map (a cost of zero is a perfect score).

4. Solve with High and Low baseline possibilities

The baseline that is used has an uncertainty. The inversion system is now solved three times, once with the mean baseline, once using the lower limit of the baseline possibility and once with the upper limit. Any systematic bias in the estimated baseline is thus considered within the uncertainty of the emission estimates.

5. New grid conforming to country outlines

As discussed in the previous section.

7 Bibliography

Manning, A. J., S. O'Doherty, A. R. Jones, P. G. Simmonds, and R. G. Derwent (2011), Estimating UK methane and nitrous oxide emissions from 1990 to 2007 using an inversion modeling approach, *J. Geophys. Res.*, **116**, D02305, doi:10.1029/2010JD014763.

8 Annex

8.1 Baseline mass mixing ratios, growth rates, seasonal cycles

(please refer to www.metoffice.gov.uk/atmospheric-trends for the latest baseline trends)

8.1.1 N_2O

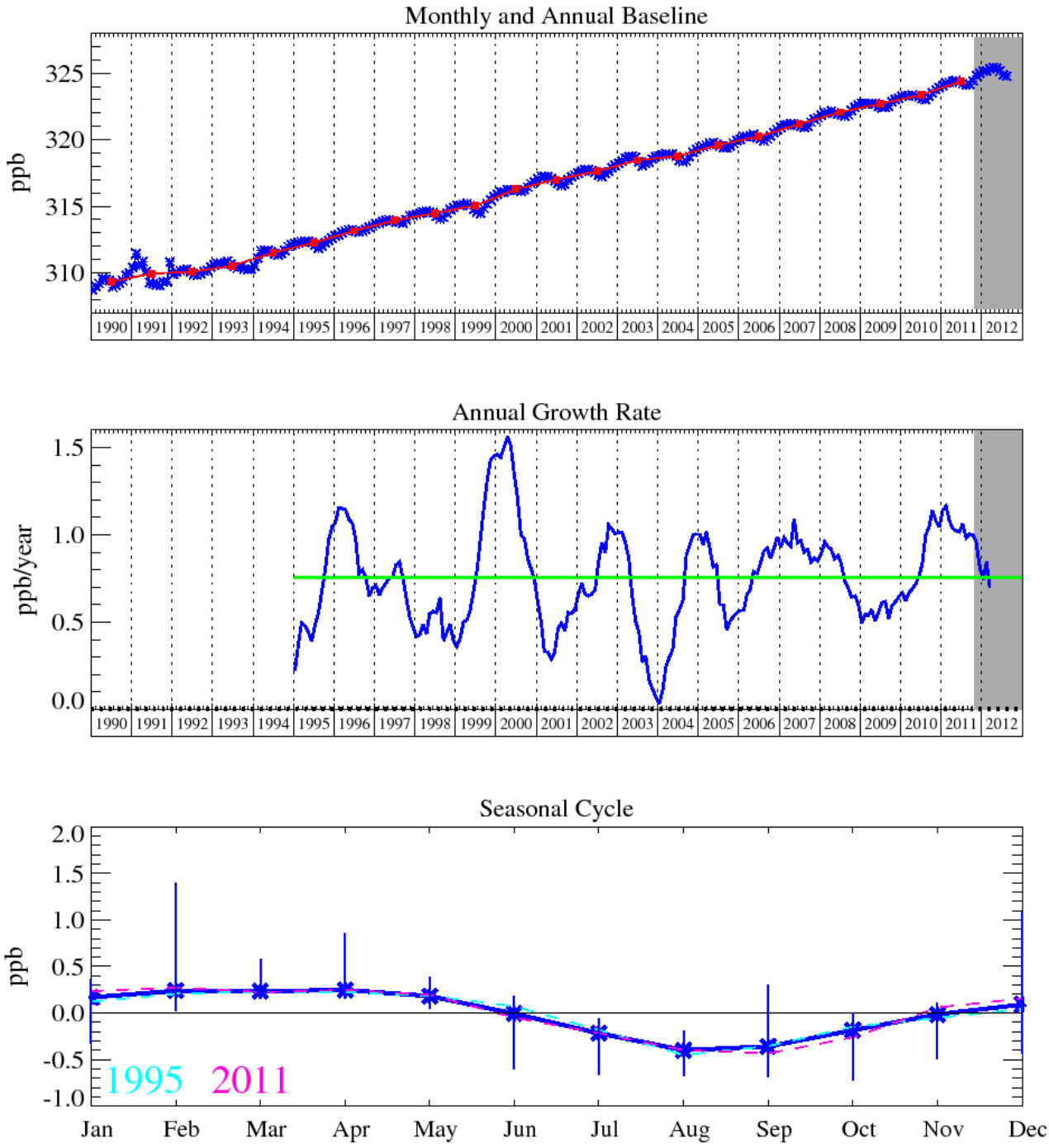

Figure 15: Top panel – Monthly (blue) and annual (red) baseline mass mixing ratios. Middle panel – Yearly (blue) and overall (green) baseline growth rate. Lower panel – Seasonal cycle (de-trended) with year to year variability. Grey area shows unratified data period.

8.1.2 CH4

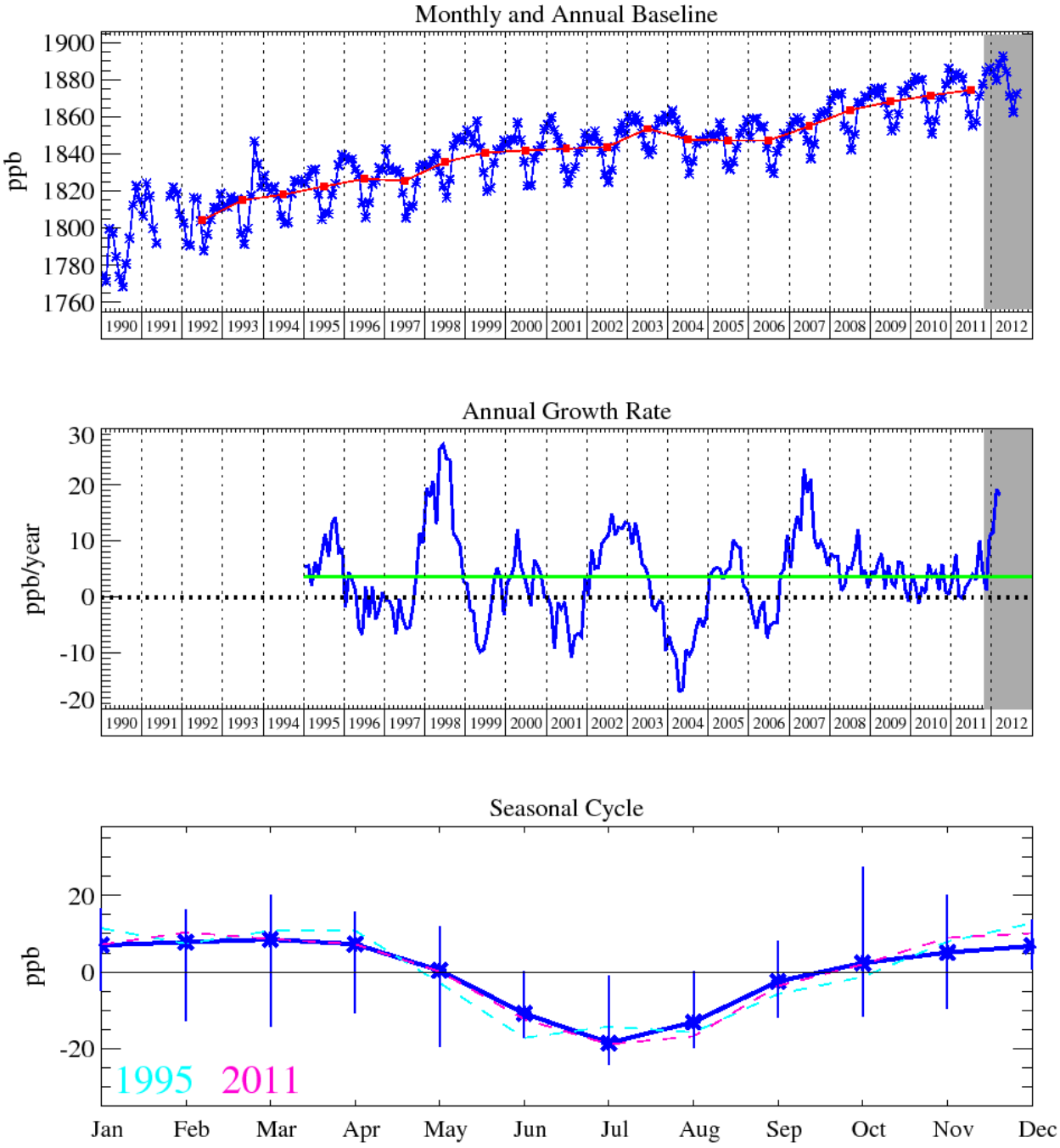

Figure 16: Top panel – Monthly (blue) and annual (red) baseline mass mixing ratio. Middle panel – Yearly (blue) and overall (green) baseline growth rate. Lower panel – Seasonal cycle (de-trended) with year to year variability. Grey area shows unratified data period.

8.1.3 CFC-11

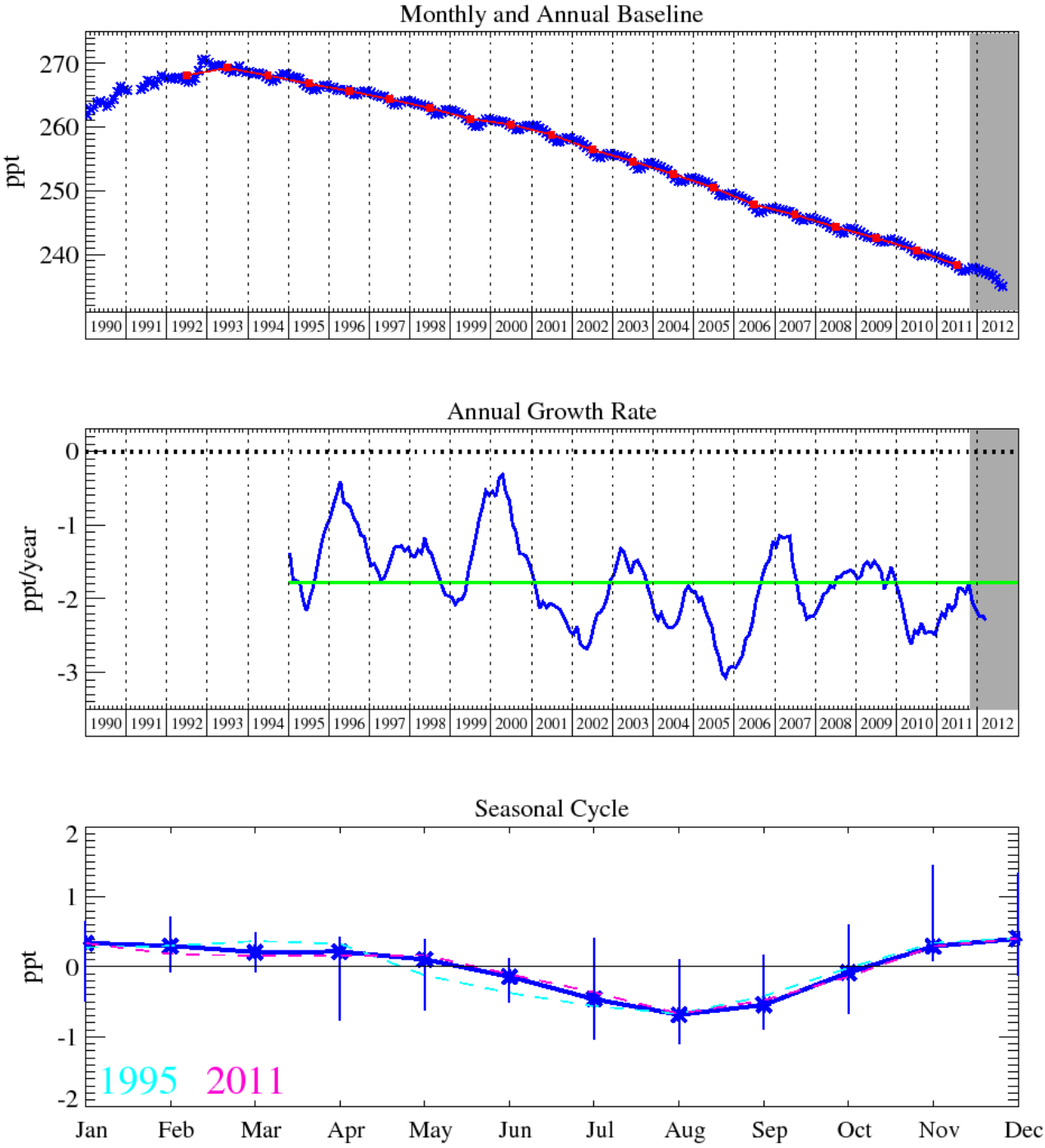

Figure 17: Top panel – Monthly (blue) and annual (red) baseline mass mixing ratio. Middle panel – Yearly (blue) and overall (green) baseline growth rate. Lower panel – Seasonal cycle (de-trended) with year to year variability. Grey area shows unratified data period.

8.1.4 HFC-134a

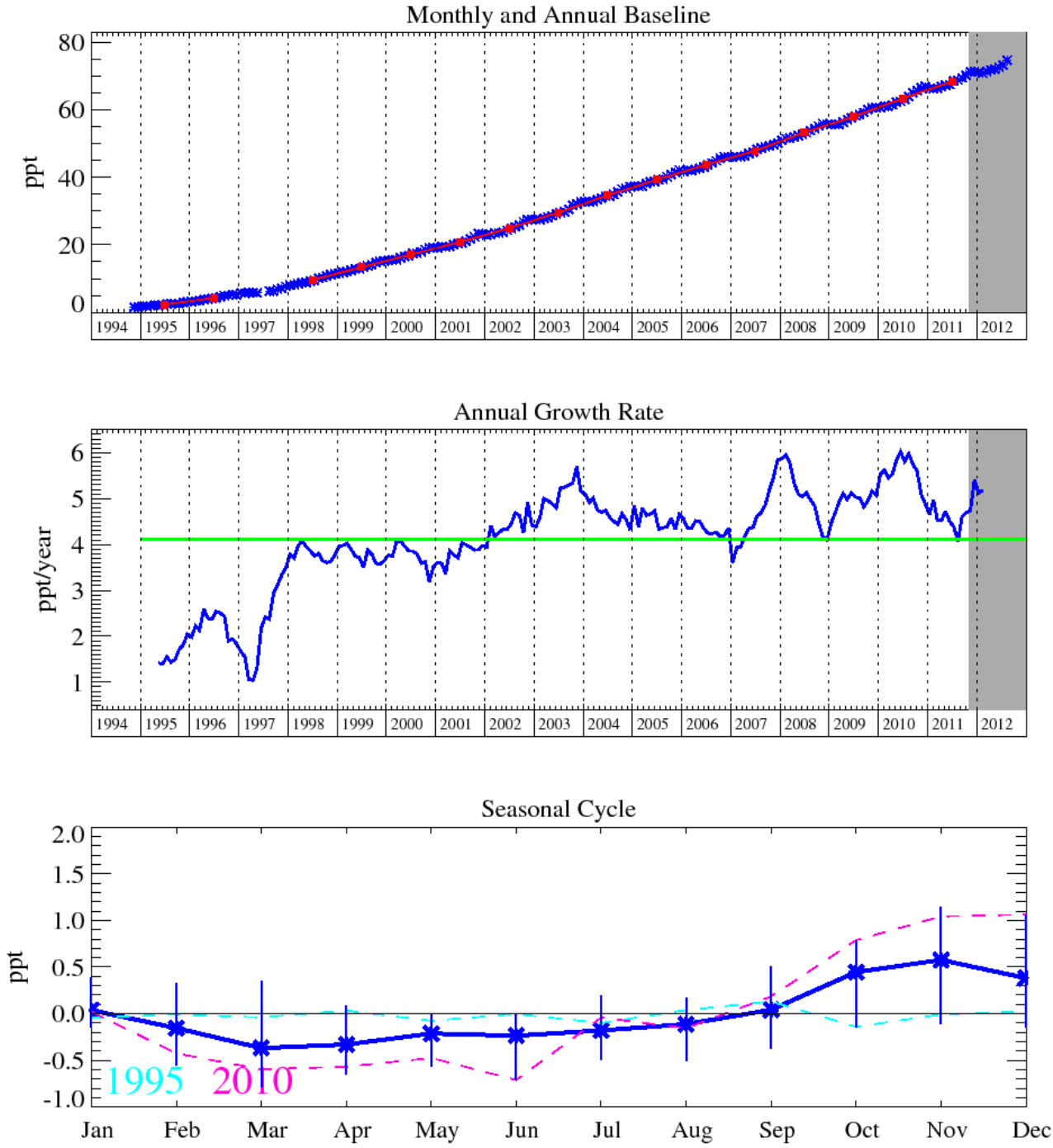

Figure 18: Top panel – Monthly (blue) and annual (red) baseline mass mixing ratio. Middle panel – Yearly (blue) and overall (green) baseline growth rate. Lower panel – Seasonal cycle (de-trended) with year to year variability. Grey area shows unratified data period.

8.1.5 HFC-125

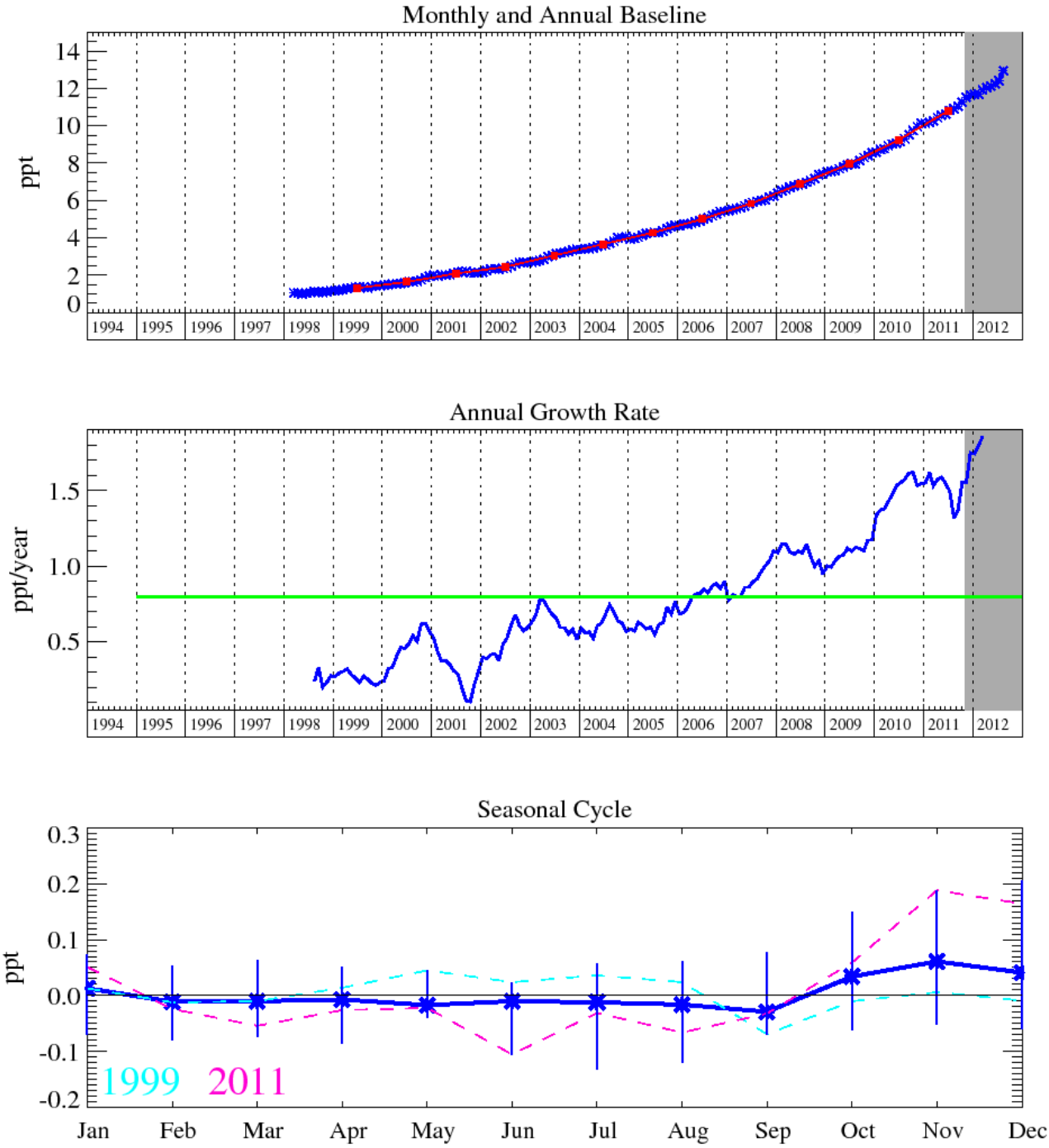

Figure 19: Top panel – Monthly (blue) and annual (red) baseline mass mixing ratio. Middle panel – Yearly (blue) and overall (green) baseline growth rate. Lower panel – Seasonal cycle (de-trended) with year to year variability. Grey area shows unratified data period.

8.1.6 HFC-143a

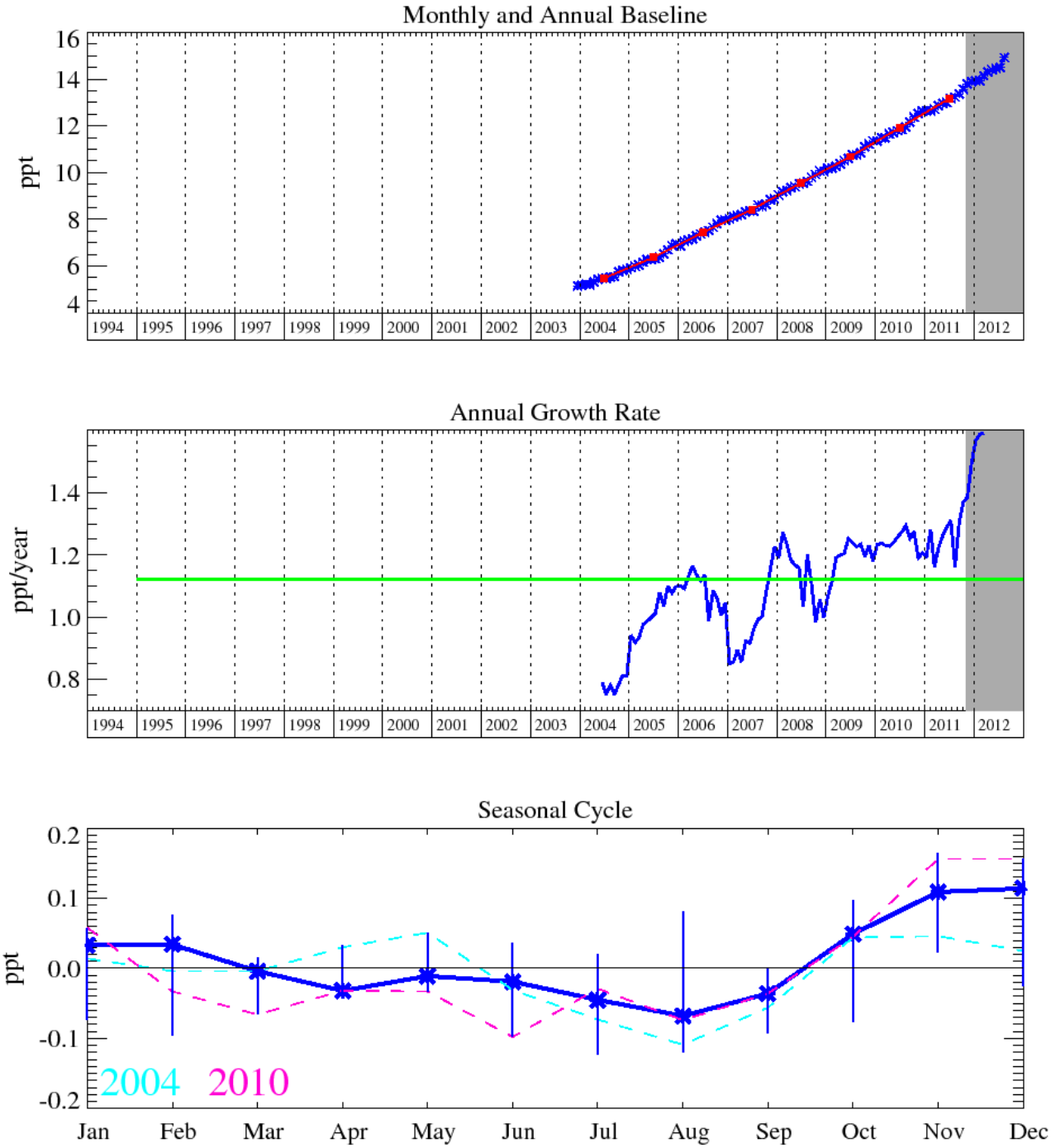

Figure 20: Top panel – Monthly (blue) and annual (red) baseline mass mixing ratio. Middle panel – Yearly (blue) and overall (green) baseline growth rate. Lower panel – Seasonal cycle (de-trended) with year to year variability. Grey area shows unratified data period.

8.1.7 HFC-32

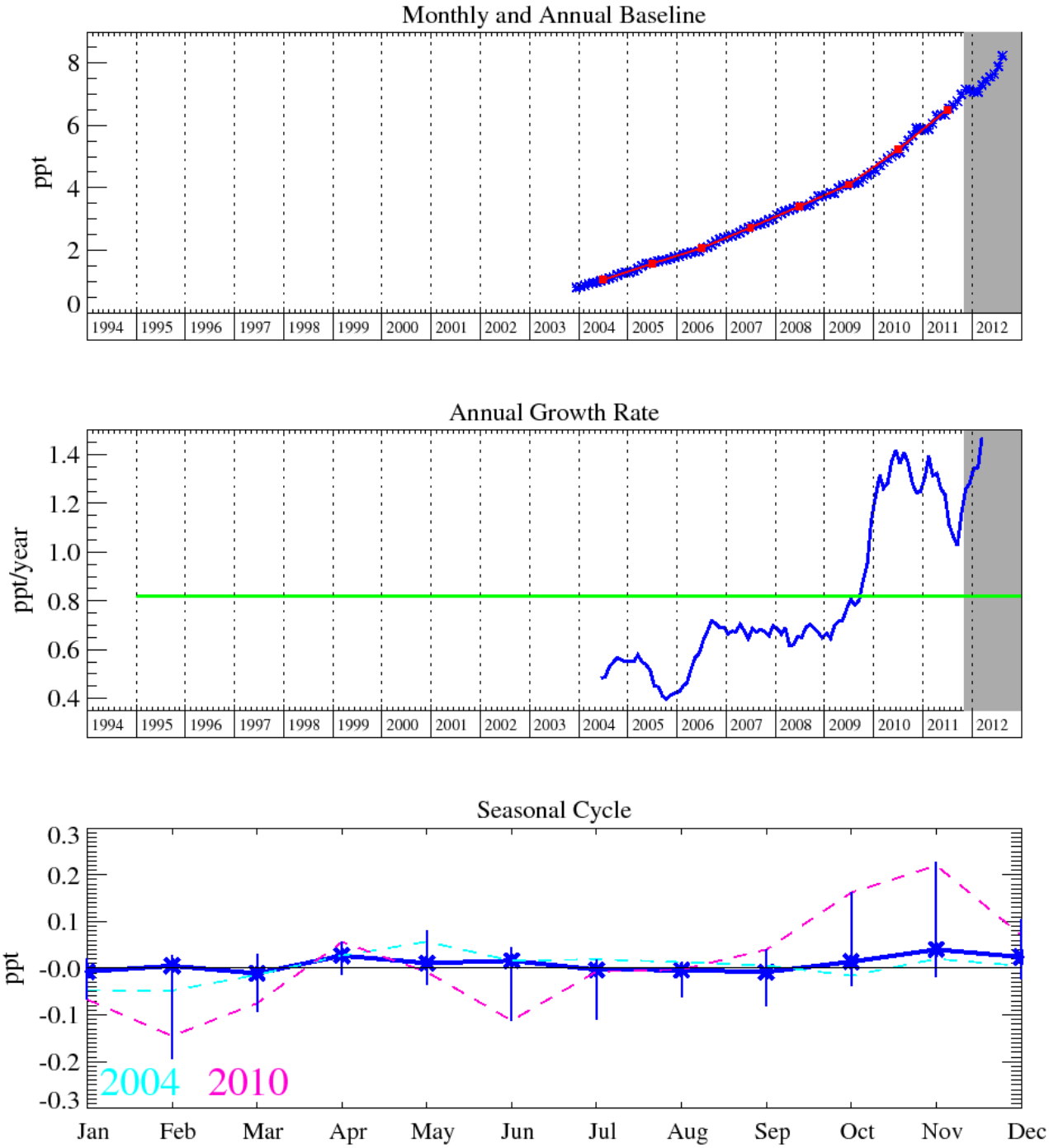

Figure 21: Top panel – Monthly (blue) and annual (red) baseline mass mixing ratio. Middle panel – Yearly (blue) and overall (green) baseline growth rate. Lower panel – Seasonal cycle (de-trended) with year to year variability. Grey area shows unratified data period.

8.1.8 HFC-152a

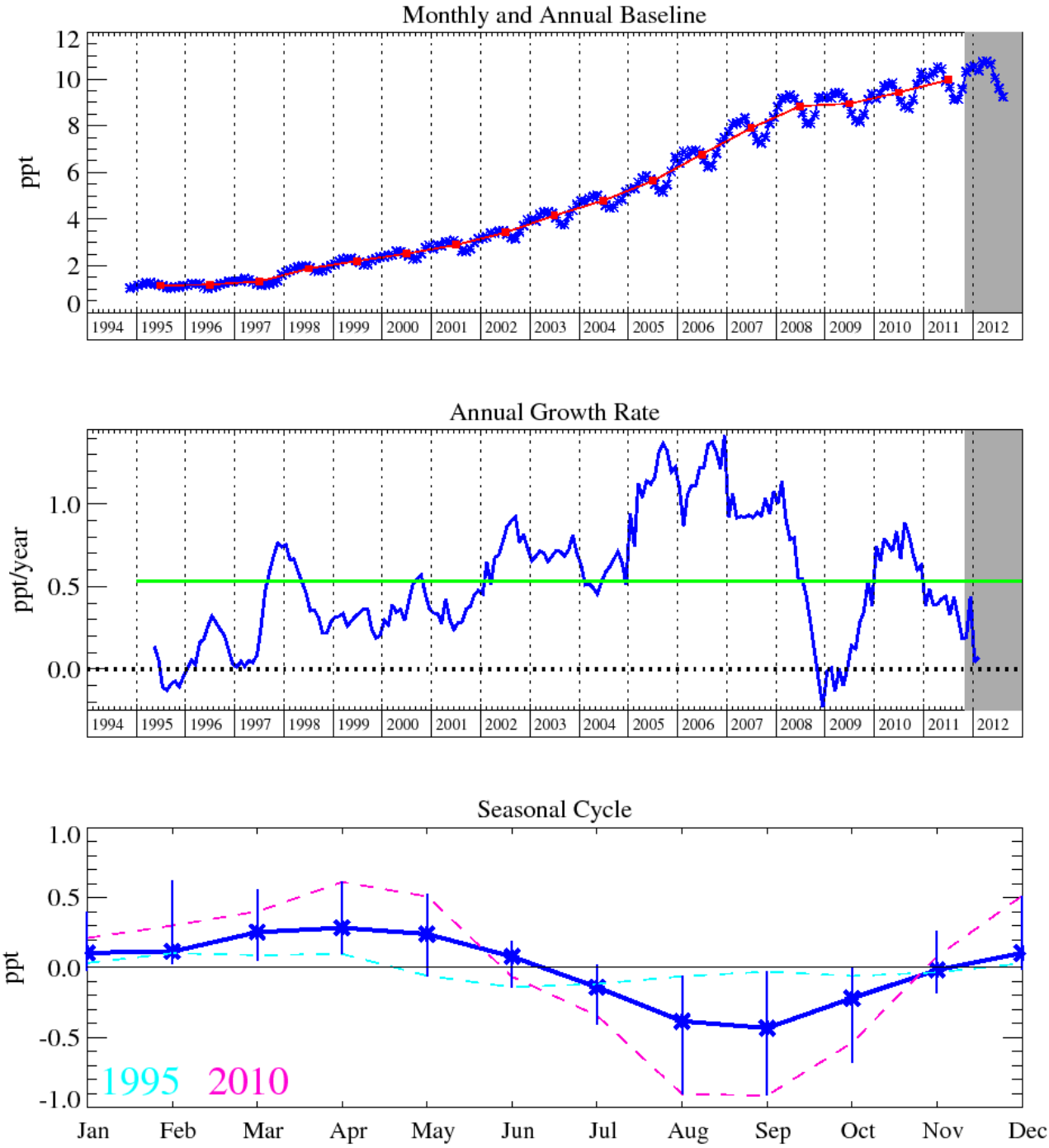

Figure 22: Top panel – Monthly (blue) and annual (red) baseline mass mixing ratio. Middle panel – Yearly (blue) and overall (green) baseline growth rate. Lower panel – Seasonal cycle (de-trended) with year to year variability. Grey area shows unratified data period.

8.1.9 HFC-23

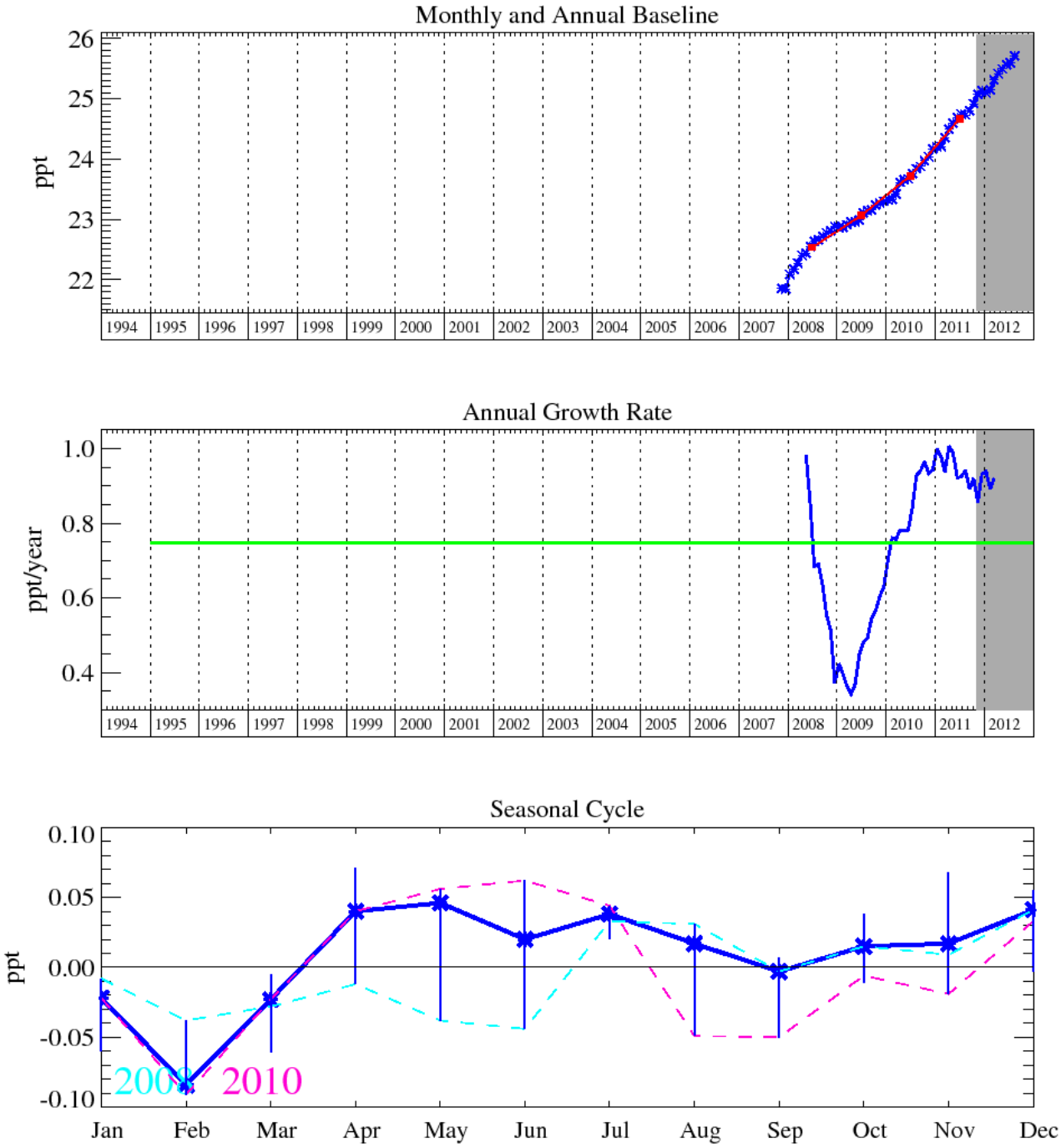

Figure 23: Top panel – Monthly (blue) and annual (red) baseline mass mixing ratio. Middle panel – Yearly (blue) and overall (green) baseline growth rate. Lower panel – Seasonal cycle (de-trended) with year to year variability. Grey area shows unratified data period.

8.1.10 HCFC-141b

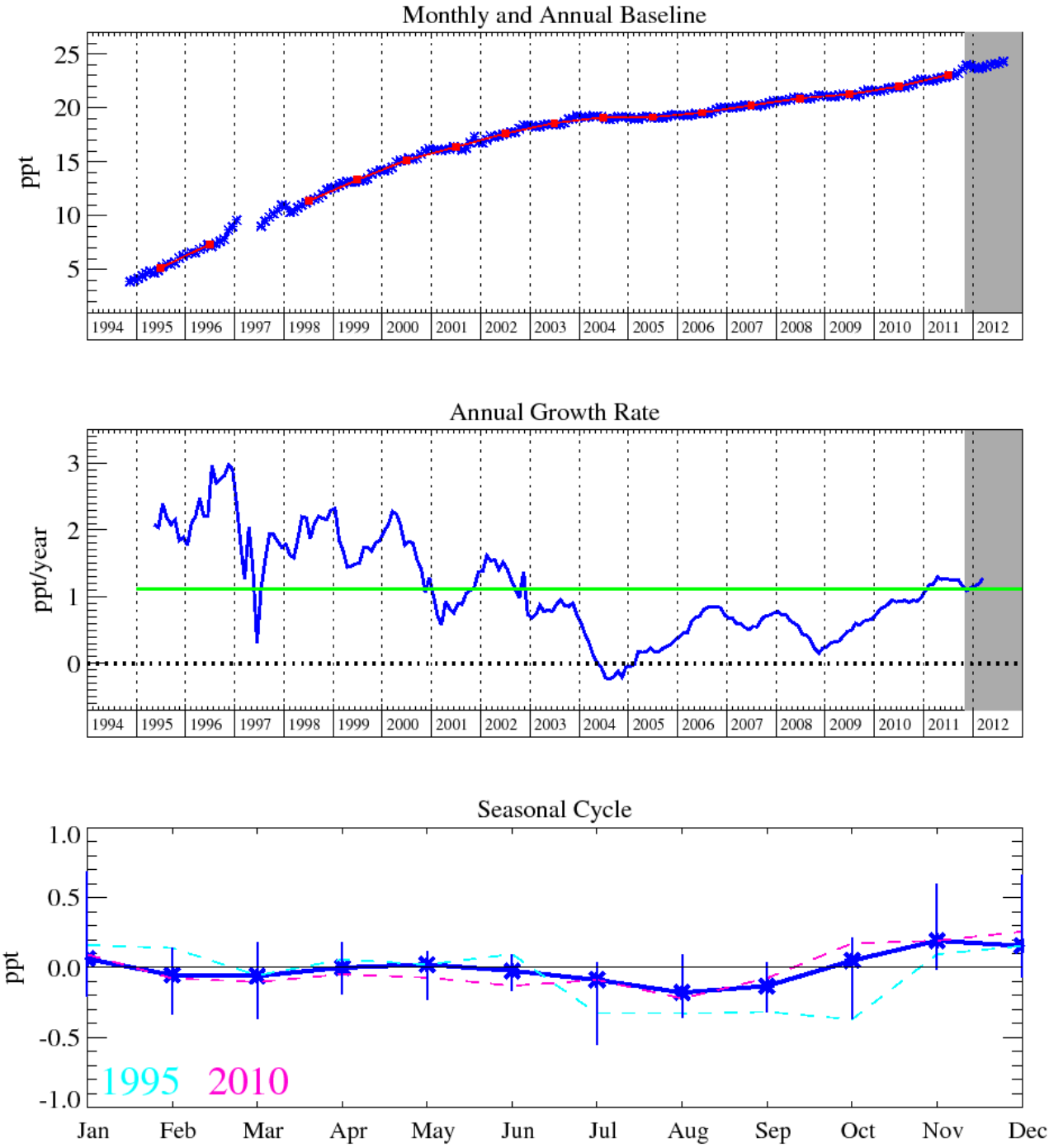

Figure 24: Top panel – Monthly (blue) and annual (red) baseline mass mixing ratio. Middle panel –Yearly (blue) and overall (green) baseline growth rate. Lower panel – Seasonal cycle (de-trended) with year to year variability. Grey area shows unratified data period.

8.1.11 HCFC-22

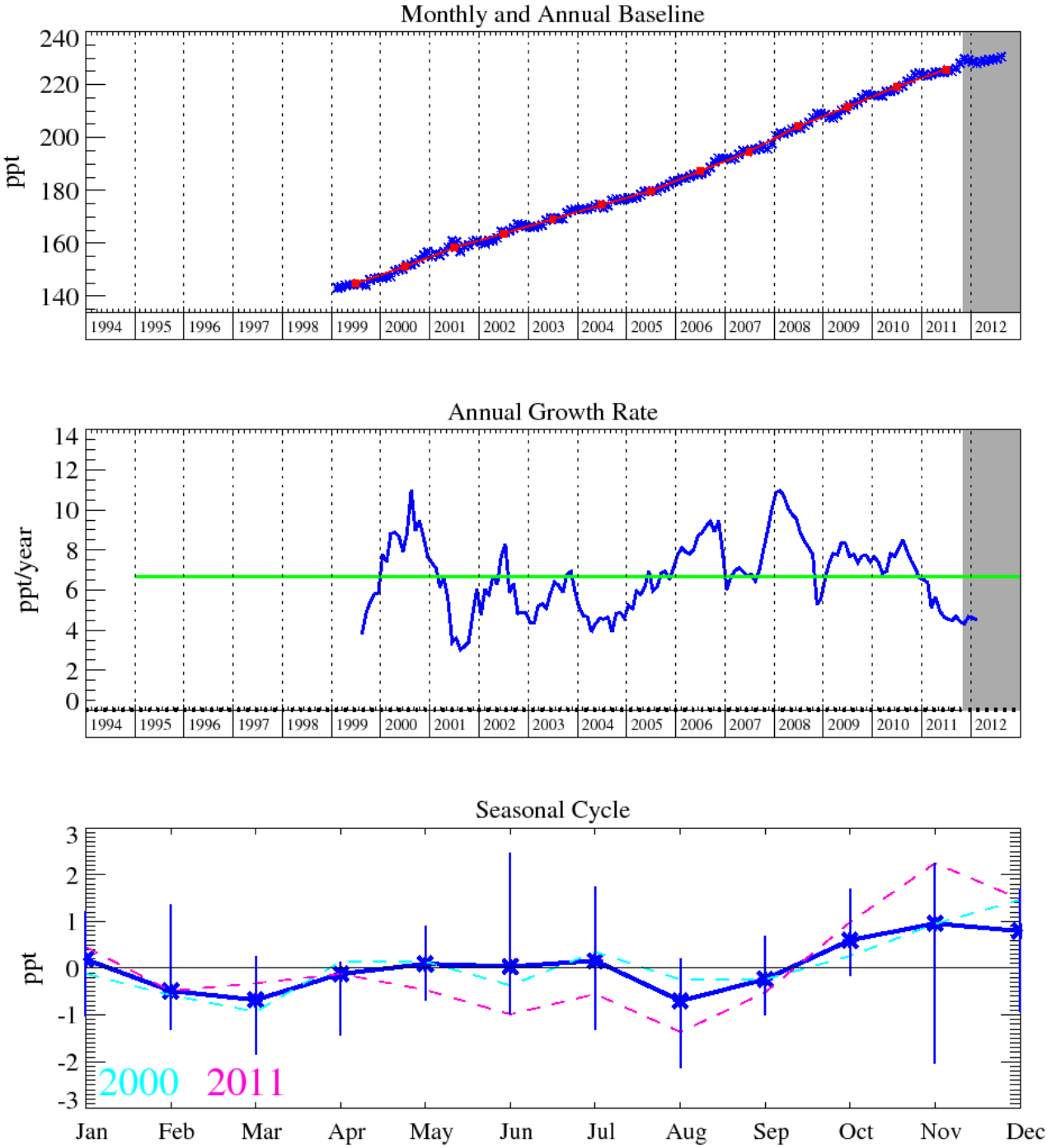

Figure 25: Top panel – Monthly (blue) and annual (red) baseline mass mixing ratio. Middle panel – Yearly (blue) and overall (green) baseline growth rate. Lower panel – Seasonal cycle (de-trended) with year to year variability. Grey area shows unratified data period.